

Electronic Correlation and Geometrical Frustration in Molecular Solids – A Systematic *ab initio* Study of β' - $X[\text{Pd}(\text{dmit})_2]_2$

Takahiro Misawa^{1,†}, Kazuyoshi Yoshimi^{1,†} and Takao Tsumuraya²

¹*Institute for Solid State Physics, University of Tokyo,
5-1-5 Kashiwanoha, Kashiwa, Chiba 277-8581, Japan*

²*Priority Organization for Innovation and Excellence,
Kumamoto University, 2-39-1 Kurokami, Kumamoto 860-8555, Japan and*

[†]The authors contributed to this work equally.

(Dated: September 15, 2020)

We systematically derive low-energy effective Hamiltonians for molecular solids β' - $X[\text{Pd}(\text{dmit})_2]_2$ (X represents a cation) using *ab initio* density functional theory calculations and clarify how the cation controls the inter-dimer transfer integrals and the interaction parameters. The effective models are solved using the exact diagonalization method and the antiferromagnetic ordered moment is shown to be significantly suppressed around the spin-liquid candidate of $X=\text{EtMe}_3\text{Sb}$, which is reported in experiments. We also show that both the geometrical frustration and the off-site interactions play essential roles in the suppression of antiferromagnetic ordering. This systematic derivation and analysis of the low-energy effective Hamiltonians offer a firm basis to clarify the nature of the quantum spin liquid found in β' - $\text{EtMe}_3\text{Sb}[\text{Pd}(\text{dmit})_2]_2$.

Introduction— Quantum spin liquids (QSLs) [1], which are Mott insulators without any broken symmetry, even at zero temperature, are new states of matter that have attracted much interest in the last few decades. In pioneering work by Anderson and Fazekas [2, 3], it was proposed that geometrical frustration in the magnetic interactions can melt magnetic order and induce a QSL. Motivated by such a proposal, much theoretical and experimental work has been done to search for QSLs in frustrated magnetic materials [1, 4, 5].

In the molecular solids, the van der Waals interactions among molecules tend to align them in a closed-packed way; therefore, they often form frustrated lattices such as an anisotropic triangular lattice [6, 7]. Due to this feature, several families of molecular solids offer promising platforms for realizing QSLs, such as κ -(BEDT-TTF) $_2X$ and β' - $X[\text{Pd}(\text{dmit})_2]_2$, where X represents anion and cation species, respectively [BEDT-TTF = bis(ethylenedithio)tetrathiafulvalene, dmit = 1,3-dithiole-2-thione-4,5-dithiolate]. It was reported that no clear symmetry breaking in κ -(BEDT-TTF) $_2\text{Cu}_2(\text{CN})_3$ occurred down to 32 mK [8], which indicates that a QSL due to geometrical frustration realizes in this compound. QSLs have been discovered in several other molecular solids such as β' - $\text{EtMe}_3\text{Sb}[\text{Pd}(\text{dmit})_2]_2$ ($\text{Et} = \text{C}_2\text{H}_5$, $\text{Me} = \text{CH}_3$) [9, 10] and κ - $\text{H}_3(\text{Cat-EDT-TTF})_2$, where Cat-EDT-TTF is ethylenedithio-tetrathiafulvalene [11].

Among several QSLs found in molecular solids, $\text{Pd}(\text{dmit})_2$ salts offer an ideal platform for examining the key parameters that induce the QSL because it is possible to tune the ground states from the ordered states (antiferromagnetic ordering or charge ordering) to a QSL by systematically changing the cations [6]. In addition to that, because the high-quality samples with less impurities are available, detailed measurement of the thermal transport was done to clarify the nature of the QSL [12] and it was

proposed that the large thermal conductivity indicates the emergence of the exotic particle such as the spinon in the QSL. However, this result has been challenged by the recent experiments and the existence/absence of the exotic particle in the QSL is under hot debate [13–16]. Although the theoretical studies such as establishing the low-energy Hamiltonians are expected to play important role for resolving the contradiction, there are a few theoretical studies based on non-empirical methods.

In previous studies, the half-filled Hubbard model on an anisotropic triangular lattice has been obtained as an effective microscopic Hamiltonian to describe the electronic structures in $\text{Pd}(\text{dmit})_2$ salts [17–19] because the bands crossing the Fermi level are half-filled and isolated from the other bands. These bands mainly originate from the antibonding pair of the highest occupied molecular orbitals (HOMO) of the two $\text{Pd}(\text{dmit})_2$ molecules that form a dimer [6, 20–22]. A one band model with three interdimer transfer integrals reproduces the density functional theory (DFT) bands well [17, 23]. Through extended Hückel calculations and tight-binding fitting to DFT bands, the amplitudes of the geometrical frustration, i.e., the anisotropy of the transfer integrals, have been evaluated. It has thus been proposed that the geometrical frustration governs the magnetic properties of the dmit salts and that the magnetic order can be suppressed by changing the transfer integrals [6].

In contrast to the transfer integrals, information on the interaction parameters is limited, even though they play an important role in the stabilization and suppression of the magnetic order. Although the interaction parameters have been evaluated only for the QSL compound $X = \text{EtMe}_3\text{Sb}$ [17] in the studies of the dmit salts, the compound dependence and role in inducing the QSL state have yet to be clarified. We note that previous studies are limited to derive the low-energy effective Hamiltoni-

ans and it is not examined whether the low-energy effective Hamiltonians reproduce the cation dependence of the ground states in $\text{Pd}(\text{dmit})_2$ salts by solving them.

In this Letter, to clarify the microscopic origin of the cation dependence of the ground states in $\text{Pd}(\text{dmit})_2$ salts, we perform systematic *ab initio* derivations of the low-energy effective Hamiltonians, including both the transfer integrals and the interaction parameters for β' - $X[\text{Pd}(\text{dmit})_2]_2$. At present, 9 different $\text{Pd}(\text{dmit})_2$ salts with β' -type structure are synthesized because the mono-valent cations X can take three different types, i.e., MeY_4 , EtMe_2Y_2 , and EtMe_3Y , where the choice of pnictogen Y is P, As, and Sb. Through comparison with the obtained low-energy effective models, we find two trends in the parameters of the effective Hamiltonians: **1.** Hopping parameters t_c/t_a (definitions are given in Fig. 1(a)) increase in the order of P, As, Sb. **2.** Onsite Coulomb interactions U/t_a increase in the order of P, As, Sb (EtMe_3Sb is exceptional).

Furthermore, to identify how the microscopic parameters affect the magnetic properties, the obtained models are solved using exact diagonalization [24], which enable us to clarify the overall trend of the magnetic properties of the frustrated magnets [25, 26]. As a result, the trend in the compound dependence of the magnetic ordered moment is successfully reproduced and the magnetic ordered moment is found to be significantly suppressed in $X=\text{EtMe}_3\text{Sb}$, wherein the QSL state was reported experimentally. EtMe_3Sb is sandwiched between the Neel-type antiferromagnetic order and the striped antiferromagnetic order when the possibility of charge ordering is ignored. We also show that both geometrical frustration and off-site interactions play key roles in suppression of the antiferromagnetic order. The present results clarify the microscopic origin of the QSL and offer a firm basis to comprehensively understand QSLs found in molecular solids.

Ab initio derivation of effective models—. Based on *ab initio* calculations, the following single-band extended Hubbard-type Hamiltonian was obtained.

$$H = \sum_{ij,\sigma} t_{ij} (c_{i\sigma}^\dagger c_{j\sigma} + \text{h.c.}) + U \sum_i n_{i\uparrow} n_{i\downarrow} + \sum_{ij} V_{ij} N_i N_j + \sum_{ij,\sigma\rho} J_{ij} (c_{i\sigma}^\dagger c_{j\rho}^\dagger c_{i\rho} c_{j\sigma} + c_{i\sigma}^\dagger c_{i\rho}^\dagger c_{j\rho} c_{j\sigma}), \quad (1)$$

where $c_{i\sigma}^\dagger$ ($c_{i\sigma}$) is a creation (annihilation) operator of an electron with spin σ in the Wannier orbital localized at the i th dmit dimers. The number operators are defined as $n_{i\sigma} = c_{i\sigma}^\dagger c_{i\sigma}$ and $N_i = n_{i\uparrow} + n_{i\downarrow}$. We evaluate the transfer integrals t_{ij} , the on-site Coulomb interaction U , the off-site Coulomb interaction V_{ij} , and direct exchange interactions J_{ij} in an *ab initio* way. We note that the double-counting problem on the Hartree terms for the multi-orbital systems [27, 28] does not exist in this study because the employed model is the single-band model.

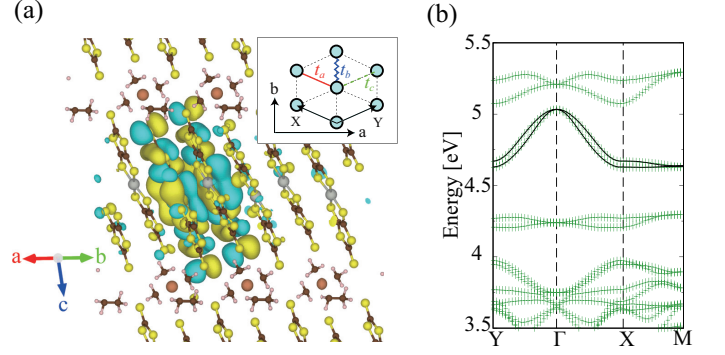


FIG. 1: (color online) (a) Wannier function for EtMe_3Sb drawn using VESTA [29]. The inset shows a schematic of the lattice structure of EtMe_3Sb in the a - b plane. Circles correspond to Wannier centers and transfer integrals between the nearest-neighbor Wannier orbitals are shown. (b) Band dispersion for EtMe_3Sb . The dotted (solid) lines are obtained by the first-principles DFT method (Wannier interpolation).

From here, we detail how to evaluate these parameters.

To derive low-energy effective Hamiltonians, we first perform non-spin-polarized calculations with a first-principles DFT method [30, 31] and obtain the Bloch functions for experimental structures of the nine members of β' -type $X[\text{Pd}(\text{dmit})_2]_2$, of which the structures are measured above the antiferromagnetic or charge ordering transition temperature [32, 33]. All the structures have the same space group symmetry of $C2/c$. The positions of all the H atoms were relaxed because those determined from x-ray diffraction measurements typically show slightly shorter C–H bond distances than the DFT optimized positions. One-electron Kohn-Sham equations are solved self-consistently using a pseudopotential technique with plane wave basis sets, which is implemented in the scalar relativistic code of **Quantum Espresso 6.3** [34]. The exchange-correlation functional used is the generalized gradient approximation (GGA) proposed by Perdew, Burke, and Ernzerhof (PBE) [35]. The cutoff energies for plane waves and charge densities were set to be 70 and 280 Ry, respectively. A $5 \times 5 \times 3$ uniform k -point mesh was used with a Gaussian smearing method during self-consistent loops.

After obtaining the Bloch functions, the maximally localized Wannier functions (MLWF) were constructed using **RESPACK** [36]. To make the MLWF, the half-filled bands crossing the Fermi level were selected as the low-energy degrees of freedom. Initial coordinates of the MLWF were set to be at the center between two $[\text{Pd}(\text{dmit})_2]$ monomers to generate a one band model (so-called dimer model) [37].

In Fig. 1(a), we show the MLWF for $X=\text{EtMe}_3\text{Sb}$. The MLWF, of which the center position is located at the center between two $[\text{Pd}(\text{dmit})_2]$ monomers, spreads over the molecule and forms the dimer unit. Figure 1(b) shows

that the MLWF nearly perfectly reproduces the band structures obtained by the DFT calculations. Using the MLWF, the transfer integrals of the low-energy effective models were evaluated as

$$t_{nm}(\mathbf{R}) = \langle \phi_{n,0} | H_k | \phi_{m,\mathbf{R}} \rangle, \quad (2)$$

where $\phi_{n,\mathbf{R}}$ is the n th MLWF centered at \mathbf{R} , and H_k is the one-body part of the *ab initio* Hamiltonian. The lattice structure in the dimer units is shown in the inset of Fig. 1(a). We note that t_a is the largest transfer integral and t_c/t_a denotes the amplitude of the geometrical frustration as discussed later.

Figure 2(a) shows the compound dependence of the normalized transfer integrals obtained by the MLWF fitting. For comparison, the transfer integrals obtained by the extended Hückel calculations are shown. Although the transfer integrals evaluated by the MLWF are slightly different from those obtained by the extended Hückel calculations, the trend of the compound dependence is consistent, i.e., t_b/t_a is not largely dependent on the cations and t_c/t_a increases in the order of P, As, and Sb. This trend is also found in the literature and the origin can be attributed to the cation radius, which controls the distortion of the dmit molecules [32].

The interactions were also evaluated by the constrained random-phase approximation (cRPA) [38] method using **RESPACK**. The energy cutoff for the dielectric function was set to be 3 Ry. The interaction terms are given as follows:

$$W_{nm,kl}(\mathbf{R}_1, \mathbf{R}_2, \mathbf{R}_3, \mathbf{R}_4) = \langle \phi_{n\mathbf{R}_1} \phi_{m\mathbf{R}_2} | H_W | \phi_{k\mathbf{R}_3} \phi_{l\mathbf{R}_4} \rangle, \quad (3)$$

where H_W represents the interaction term of the *ab initio* Hamiltonians. Although three-body and four-body interactions generally occur, we only treat the two-body interactions, such as density-density interactions $U_{mn}(\mathbf{R}) = W_{mm,nn}(\mathbf{0}, \mathbf{0}, \mathbf{R}, \mathbf{R})$ (that is, the on-site and off-site Coulomb interactions) and the direct exchange interactions $J_{mn}(\mathbf{R}) = W_{mn,nm}(\mathbf{0}, \mathbf{R}, \mathbf{R}, \mathbf{0})$ because the amplitudes of other terms are negligibly small. In [39], we show number of the screening bands dependence of the interaction parameters. We note that when the number of screening bands becomes large, the cRPA method can be valid in contrast to the previous studies [40, 41].

Figure 2(b) shows the compound dependence of the normalized onsite Coulomb interaction U/t_a . U/t_a increases in the order of P, As, Sb, as in the transfer integrals, except for EtMe₃Sb. As we have detailed in [39], the compound dependence of U/t_a is mainly controlled by changes in t_a because U is not largely dependent on the compounds. The transfer integral t_a decreases in the order of P, As, and Sb because the distortions of the molecules become larger in this order [32]. In contrast, U does not show a large compound dependence (see S.1 in [39]), and for this reason, U/t_a increases in the order of P, As, and Sb. Low-temperature structures were

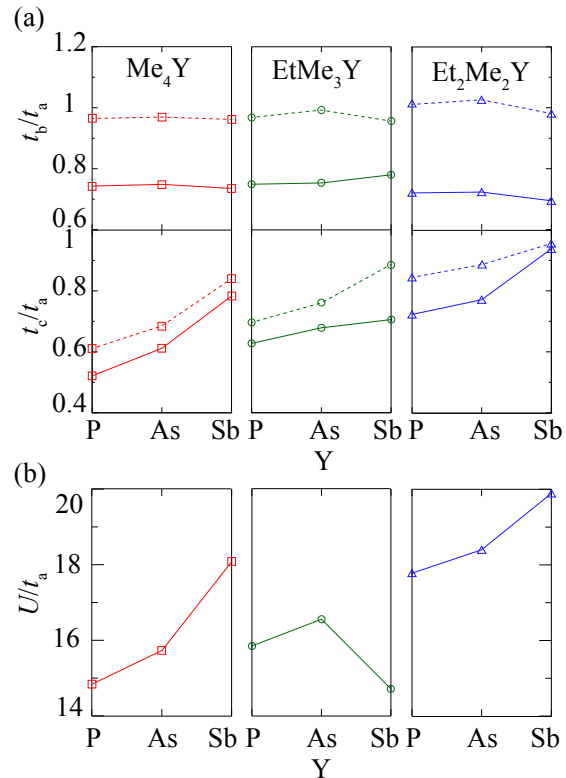


FIG. 2: (color online) (a) Band dispersion for EtMe₃Sb. The dotted (solid) lines are obtained by the first-principles DFT method (Wannier interpolation). (b) Material dependency of t_b/t_a and t_c/t_a . The dotted (solid) lines are obtained by the transfer integrals calculated by the extended Hückel method [32] (Wannier function basis).

employed for EtMe₃Sb; therefore, t_a becomes large and U/t_a becomes small. This is the origin of the exceptional behavior observed in EtMe₃Sb. We also point out that U/W (W is the band width) is estimated as $U/W \sim 2.0$ for EtMe₃Sb, which is roughly consistent with the experimental estimation ($U/W \sim 2.3$) [42].

Analysis of effective models— To clarify how the geometrical frustration and the interaction parameters affect the magnetic properties in the low-energy effective models defined in Eq. (1), exact diagonalization was performed for small clusters (system size is $N_s = 4 \times 4$ with the periodic boundary conditions). In the calculations, we take the transfer integrals, off-site Coulomb interactions, and the direct exchange interactions up to the next-nearest neighbor. Using exact diagonalization, the compound dependence of the magnetic properties can be clarified without relying on any specific approximations. It should be noted that it is necessary to introduce a constant shift in the interaction parameters to reflect the two-dimensionality of the effective models, and to obtain physically reasonable results. Following the parameter-free approach, we employ a constant shift of $\Delta = 0.30$ eV

for all compounds, which is a value comparable to that in the literature [17]. In S. 2 [39], we examine the effects of Δ and confirm that the changes in the constant shift do not change the results significantly.

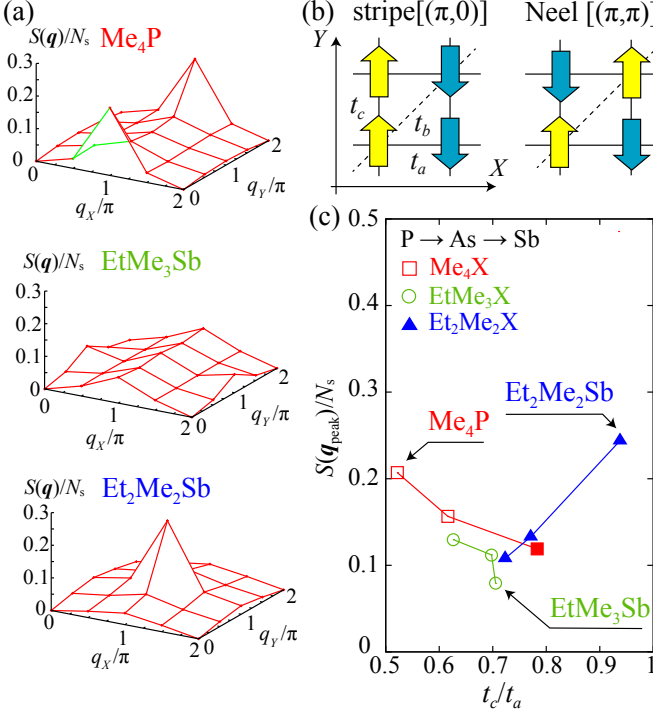


FIG. 3: (color online) (a) Spin structure factors for three typical compounds. A significant reduction of the Bragg peak occurs in EtMe_3Sb . (b) Schematic diagrams for stripe and Neel ordered states. (c) Dependence of the spin structure factors on t_c/t_a . For each family, t_c/t_a increases in the order of P, As, and Sb.

Figure 3(a) shows the spin structure factors

$$S(\mathbf{q}) = \frac{1}{N_s} \sum_{i,j} \langle \mathbf{S}_i \cdot \mathbf{S}_j \rangle e^{i\mathbf{q}(\mathbf{r}_i - \mathbf{r}_j)} \quad (4)$$

for several compounds, i.e., $X = \text{Me}_4\text{P}$, EtMe_3Sb , and $\text{Et}_2\text{Me}_2\text{Sb}$ (the spin structure factors for all nine compounds are shown in S. 3 [39]). In Me_4P , which shows the highest Neel temperature and anisotropy of transfer integrals, the spin structure factor is a sharp peak at $\mathbf{q} = (\pi, 0)$, which indicates a stripe magnetic order (top panel in Fig. 3(b)). The amplitudes of the spin structure factors are significantly suppressed in EtMe_3Sb and no clear signature of magnetic order is evident. Additionally, we note that no clear signatures of other exotic non-magnetic phases, such as the bond-order phase [43, 44], are observed (see S. 4 in [39]). This indicates that the QSL state is formed in this compound. On the other hand, for $\text{Et}_2\text{Me}_2\text{Sb}$, the sharp peak appears at $\mathbf{q} = (\pi, \pi)$, which indicates a Neel-type magnetic order shown in the bottom panel in Fig. 3(b). The ground

state is a charge ordered state [45]; therefore, this result is apparently inconsistent with previous experimental results. However, this discrepancy can be attributed to the discarding of the long-range part of the Coulomb interactions; in a 4×4 systems size, only the the Coulomb interactions up to the next-nearest neighbor can be treated, and the charge-order pattern cannot be accurately determined. We note that, it is pointed out the the interplay of the long-range Coulomb interactions and the electron-phonon couplings stabilizes the charge-ordered phase in $\text{Et}_2\text{Me}_2\text{Sb}$ [46]. Our analysis indicates that $\text{Et}_2\text{Me}_2\text{Sb}$ has antiferromagnetic instability toward (π, π) , if we ignore the instability toward charge ordering.

Figure 3(c) shows the compound dependence of the peak values of the spin structure factor $S(\mathbf{q}_{\text{peak}})$ as a function of t_c/t_a . $X = \text{EtMe}_3\text{Sb}$ is located around the boundary of the stripe and Neel magnetic order, and $S(\mathbf{q}_{\text{peak}})$ is significantly reduced at $X = \text{EtMe}_3\text{Sb}$. The overall trend of the compound dependence of the spin structure factors is consistent with the experimental results [6]. It is especially noteworthy that the low-energy effective Hamiltonian for EtMe_3Sb shows suppression of the spin structure factors, which is consistent with experimentally observed QSL behavior.

To clarify the origin of the magnetic ordered moment reduction, we systematically changed the parameters in the *ab initio* effective Hamiltonian for EtMe_3Sb . First, the effects of the geometrical frustration were examined by changing t_c/t_a . In Fig. 4(a), we show the t_c/t_a dependence of $S(\mathbf{q}_{\text{peak}})$. By artificially decreasing t_c/t_a , a sudden change in $S(\mathbf{q}_{\text{peak}})$ occurs at $t_c/t_a \sim 0.58$, which indicates a first-order phase transition between the stripe magnetic ordered phase and the possible QSL state. This result clearly shows that the geometrical frustration plays a key role in suppression of the magnetic ordered moment.

Next, we introduce λ , which monotonically scales the off-site interactions including the off-site Coulomb interactions (V_{ij}) and the direct exchange interactions (J_{ij}), i.e., (V_{ij}, J_{ij}) is scaled as $(\lambda V_{ij}, \lambda J_{ij})$. Note that $\lambda = 1$ corresponds to the *ab initio* Hamiltonian and $\lambda = 0$ corresponds to the simple Hubbard model that has only on-site Coulomb interactions U . The dependence of $S(\mathbf{q}_{\text{peak}})$ on λ is shown in Fig. 4(b). $S(\mathbf{q}_{\text{peak}})$ increases by decreasing λ , and the stripe magnetic order appeared below $\lambda = 0.5$ (the spin structure factor at $\lambda = 0$ is shown in the inset). This result indicates that the off-site interactions, which are often ignored in the previous studies, suppress the magnetic ordered moment and play an important role in the stabilization of the QSL state in $\text{Pd}(\text{dmit})_2$ salts. We note that both V_{ij} and J_{ij} reduce the magnetic ordered moment (see S. 5 in [39]). The mechanism of the reduction can be attributed to the reduction of U and resultant enhancement of the higher-order interactions such as the ring-exchange interactions, which suppress the magnetic

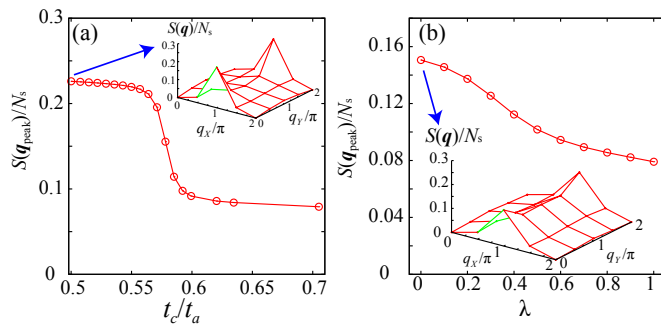


FIG. 4: (color online) (a) Dependence of $S(\mathbf{q}_{\text{peak}})$ on t_c/t_a . Around $t_c/t_a \sim 0.57$, the stripe magnetic correlations suddenly increase. The inset shows the spin structure factors at $t_c/t_a = 0.5$, which indicate the stripe magnetic order. (b) Dependence of the peak value of the spin structure factors on λ for $X=\text{EtMe}_3\text{Sb}$. The inset shows the spin structure factors at $\lambda = 0$.

long-range orders [47–49].

Summary— To conclude, we have successfully reproduced the overall trend in the magnetic properties by performing comprehensive *ab initio* calculations for all available β' -type $\text{Pd}(\text{dmit})_2$ salts. An antiferromagnetic order with a stripe pattern becomes the ground state for small t_c/t_a such as Me_4P . This result is consistent with experimental results that the Neel temperatures increase with decreasing t_c/t_a . However, the magnetic ordered moment is significantly suppressed around EtMe_3Sb . These results indicate that the QSL state without magnetic order appears in EtMe_3Sb , which is consistent with previous experimental results. We have also shown that cooperation of the geometrical frustration and the off-site interactions induce suppression of the magnetic ordered moment in EtMe_3Sb . To analyze the QSL state in molecular solids, most theoretical calculations have been conducted for frustrated Hubbard models that only have on-site Coulomb interactions [19, 50, 51]. The present *ab initio* calculations, which suggest the importance of the off-site interactions, require reconsideration of the use of such simple models to describe the QSL state in $\text{Pd}(\text{dmit})_2$ salts.

Analysis of the low-energy effective model in this Letter is limited to small system sizes in order to perform an exact analysis to clarify the general trend in the $\text{Pd}(\text{dmit})_2$ salts. Several highly accurate wavefunction methods for the strongly correlated electron systems have recently been developed [52–54]. The clarification of the possible exotic elementary excitation of the QSL state in EtMe_3Sb using such cutting edge methods, which is a hotly debated issue in experiments [12–14, 16], is a significant challenge but left for future studies. We also note that the applications of the employed *ab initio* method to other families of the molecular solids such as κ -ET salts will help us to comprehensively understand the nature of

the QSL found in other compounds [55].

The calculations were partly conducted at the Supercomputer Center, Institute for Solid State Physics, University of Tokyo. This work was supported by Kakuhhi Grants-in-Aid (Nos. JP16H06345, JP19K03739, and 19K21860) from the Japan Society for the Promotion of Science (JSPS). The authors thank Kazuma Nakamura for useful discussions on RESPACK. The authors thank Reizo Kato for stimulating discussion on the experimental aspects of the materials. T.M. and K.Y. thank Hiroshi Shinaoka for a discussion on the cRPA. T.M. and K.Y. were also supported by the Building of Consortia for the Development of Human Resources in Science and Technology from the Ministry of Education, Culture, Sports, Science and Technology (MEXT) of Japan. T.T. was partially supported by the Leading Initiative for Excellent Young Researchers (LEADER) from MEXT of Japan. This work was supported by MEXT as “Program for Promoting Researches on the Supercomputer Fugaku” (Basic Science for Emergence and Functionality in Quantum Matter –Innovative Strongly-Correlated Electron Science by Integration of “Fugaku” and Frontier Experiments–, Project ID:hp200132).

Supplemental Material for “Electronic Correlation and Geometrical Frustration in Molecular Solids – A Systematic *ab initio* Study of β' - $X[\text{Pd}(\text{dmit})_2]_2$ ”

S.1 DOWNFOLDING RESULTS

The derived interdimer transfer integrals, and both on-site and inter-site Coulomb interaction parameters obtained by constrained Random Phase Approximation (cRPA) of β' - $X[\text{Pd}(\text{dmit})_2]_2$ are listed in Table. I. The simple transfer integrals reproduce the DFT bands for all the $\text{Pd}(\text{dmit})_2$ salts well. In general, the values of on-site and inter-site Coulomb interactions obtained by cRPA depend on the total number of bands n_b contributing to the screening. Figure 5 shows n_b -dependence of on-site and inter-site Coulomb interaction for $\text{Et}_2\text{Me}_2\text{Sb}$ salt (we select this salt, since it has the largest value of on-site Coulomb interaction in $\text{Pd}(\text{dmit})_2$ salts). With increasing n_b , both on-site and inter-site Coulomb interactions decreases and approach to the constant value. In our manuscript, n_b is set as 600.

Figure 6 shows the cation dependence of the transfer integrals t_a , and the on-site Coulomb interactions, U . The following aspects are noted. Among the parameters for the experimental structures measured at room temperature, t_a decreases in the order of P, As, and Sb. For the EtMe_3Sb salt, the distance between dimers, $[\text{Pd}(\text{dmit})_2]_2$, becomes shorter with decreasing temperature, and thus t_a become larger, and the anisotropy among three transfer integrals increases. In contrast, the cation dependence of the on-site interaction U is weak compared to that of t_a .

Experimentally, the EtMe_3Sb salt does not show the phase transition down to the lowest temperature (~ 32 mK), while the other compounds show phase transitions such as the antiferromagnetic transition and the charge ordering transition. To obtain the effective model with no ordered patterns, we adopt the crystal data of EtMe_3Sb salt at 4 K for the downfolding calculation, while for the other compounds, we adopt those obtained at room temperature.

S.2 DIMENSIONAL DOWNFOLDING

Here, we explain the effects of dimensional downfolding. The models that have three-dimensional interactions are obtained by performing constrained random phase approximation (cRPA). To reflect the two-dimensionality of the organic solids and reduce numerical costs, it is better to directly treat the two-dimensional model. To do so, Nakamura *et al.* proposed a dimensional down-

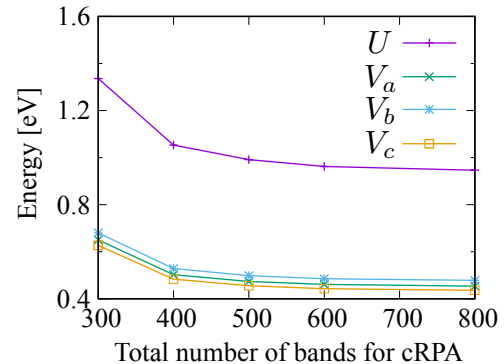


FIG. 5: (color online) Total number of bands for cRPA dependence of the on-site and inter-site Coulomb interactions for $\text{Et}_2\text{Me}_2\text{Sb}$ salt.

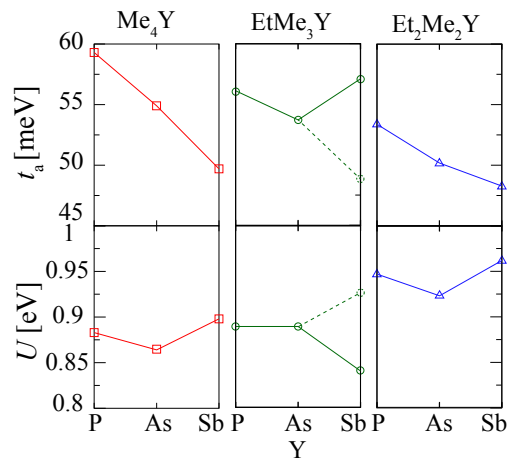


FIG. 6: (color online) Cation dependence of the transfer integrals t_a and the on-site Coulomb interactions U . The solid (dotted) symbols for the EtMe_3Sb salt show the data calculated using the x-ray structure at 4 K (room temperature).

folding method [17, 56], which renormalizes the three-dimensional interactions into two-dimensional interactions. As a result, it is shown that the dimensional downfolding simply induces a constant shift of the Coulomb interaction, irrespective of the distance, i.e.,

$$\tilde{V}_{ij} = V_{ij} - \Delta. \quad (5)$$

The amplitudes of the constant shifts are evaluated as $\Delta = 0.18$ eV for the dmit salt (EtMe_3Sb) and $\Delta = 0.2$ eV for κ -(BEDT-TTF) salt [17]. For $\Delta \geq 0.3$, \tilde{V}_{ij} for [-11] direction becomes negative for several compounds. In those cases, we simply ignore them, i.e., we set the small but finite $\tilde{V}_{ij} < 0$ as 0.

We examine the effects of the dimensional downfolding, i.e., how the constant shift Δ affects the electronic structures in the low-energy effective model. By changing Δ ,

Cation	Temperature	t_a [meV]	t_b [meV]	t_c [meV]	U [eV]	V_a [eV]	V_b [eV]	V_c [eV]	J_a [meV]	J_b [meV]	J_c [meV]
Me ₄ P	rt	59.3	44.0	30.9	0.883	0.449	0.465	0.413	3.26	2.54	1.29
Me ₄ As	rt	54.9	41.5	33.8	0.864	0.426	0.442	0.394	2.77	2.37	1.35
Me ₄ Sb	rt	49.7	36.5	38.9	0.898	0.429	0.444	0.402	2.67	1.75	1.49
EtMe ₃ P	rt	56.1	42.0	35.0	0.889	0.442	0.460	0.411	2.88	2.02	1.48
EtMe ₃ As	rt	53.7	40.9	37.2	0.889	0.436	0.456	0.409	2.60	1.84	1.45
EtMe ₃ Sb	rt	48.8	35.6	41.7	0.906	0.427	0.449	0.406	3.21	2.23	1.40
EtMe ₃ Sb	4K	57.1	44.6	40.3	0.840	0.413	0.434	0.390	2.23	1.64	1.71
Et ₂ Me ₂ P	rt	53.4	38.5	38.6	0.947	0.478	0.497	0.450	2.51	2.32	1.43
Et ₂ Me ₂ As	rt	50.2	36.3	38.7	0.923	0.422	0.467	0.448	3.30	2.63	1.73
Et ₂ Me ₂ Sb	rt	48.3	33.5	45.3	0.962	0.461	0.485	0.443	2.41	1.77	1.58

TABLE I: List of the parameters obtained by the downfolding method in the dimer-model extended Hubbard-type Hamiltonian for β' -X[Pd(dmit)₂]₂ (rt represents room temperature).

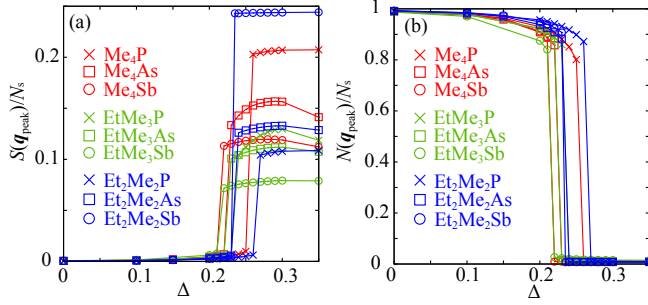


FIG. 7: (color online) (a) Dependence of the spin structure factors on Δ for 9 compounds. (b) Dependence of the charge structure factors on Δ for 9 compounds.

the effective models are solved using exact diagonalization [24]. In Fig. 7, we show the dependence of the spin and charge structure factors on Δ , which are defined as

$$S(\mathbf{q}) = \frac{1}{N_s} \sum_{i,j} \langle \mathbf{S}_i \cdot \mathbf{S}_j \rangle e^{i\mathbf{q} \cdot (\mathbf{r}_i - \mathbf{r}_j)} \quad (6)$$

$$N(\mathbf{q}) = \frac{1}{N_s} \sum_{i,j} \langle (N_i - \langle N_i \rangle)(N_j - \langle N_j \rangle) \rangle e^{i\mathbf{q} \cdot (\mathbf{r}_i - \mathbf{r}_j)} \quad (7)$$

The charge order state becomes the ground state for $\Delta = 0$ for all 9 compounds (that is, the ordering vector for the charge ordered state is $(\pi, 0)$). As Δ is increased, a discontinuous phase transition occurs between the charge order state and the antiferromagnetic states around $\Delta_{tr} = 0.2 - 0.26$ eV. The compound dependence of the transition points is shown in Fig. 8.

To perform a parameter-free approach and examine the magnetic properties of the Pd(dmit)₂ salts, $\Delta = 0.3$ was employed in this paper. Although this value is slightly larger than that obtained by previous studies, the magnetic properties are not largely dependent on Δ in the magnetic ordered phase, as shown in Fig. 7(a). Therefore, this constant shift does not significantly change the result.

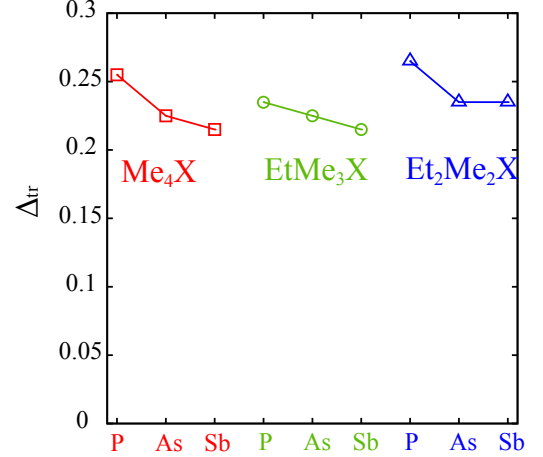


FIG. 8: (color online) Compound dependence of the transition value of Δ (Δ_{tr}).

S.3 COMPOUND DEPENDENCE OF SPIN STRUCTURE FACTORS

Although the spin structure factors for three typical compounds are shown in the main text, for comparison, we show the spin structures for all 9 compounds in Fig. 9. For Me_4P , the stripe magnetic correlations are dominant. This stripe order is suppressed by changing the cation, i.e., by increasing t_c/t_a , and a non-magnetic phase is apparent around EtMe_3Sb . For $\text{Et}_2\text{Me}_2\text{Sb}$, the Neel magnetic correlation becomes dominant because it is close to the square lattice $t_c/t_a \sim 0.8$.

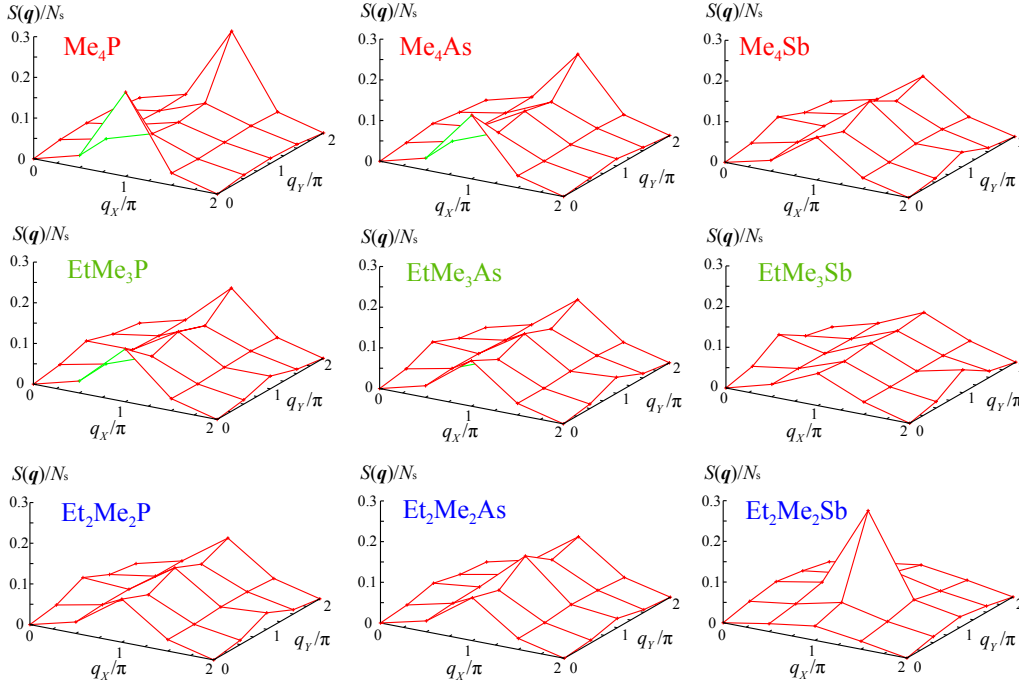


FIG. 9: (color online) Compound dependence of the spin structure factors.

S.4 BOND-ORDER STRUCTURE FACTORS

One of the possible candidates for a non-magnetic phase in the extended Hubbard model is the bond-order phase, which becomes a ground state in the one-dimensional extended Hubbard model [43, 44]. The bond-order structure factors were calculated for the low-energy effective model of EtMe₃Sb, which is defined as

$$B^e(\mathbf{q}) = \frac{1}{N_s} \sum_{i,j} \langle (B_i^e - \langle B_i^e \rangle) (B_j^e - \langle B_j^e \rangle) \rangle e^{i\mathbf{q} \cdot (\mathbf{r}_i - \mathbf{r}_j)} \quad (8)$$

$$B_i^e = \frac{1}{2} \sum_{\sigma} (c_{i+\mathbf{e},\sigma}^{\dagger} c_{i,\sigma} + c_{i,\sigma}^{\dagger} c_{i+\mathbf{e},\sigma}), \quad (9)$$

where \mathbf{e} represents the direction of the bond-order. Figure 10 shows the bond-order structure factors in the low-energy effective model for EtMe₃Sb. No clear signature of the bond order was evident.

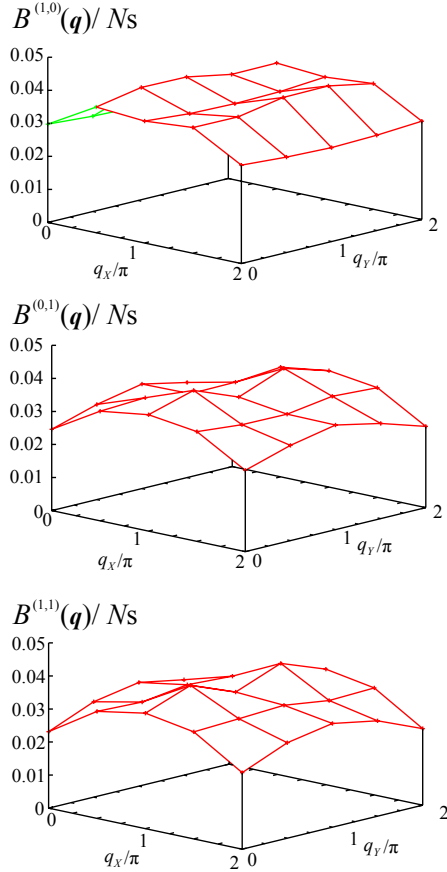


FIG. 10: (color online) Bond-order structure factors for the low-energy effective model of EtMe₃Sb. We take $\mathbf{e} = (1, 0)$, $(0, 1)$, and $(1, 1)$.

S.5 EFFECTS OF OFF-SITE INTERACTIONS

To examine the effects of the off-site Coulomb interactions and the direct exchange interactions separately, we introduce the scaling parameters λ_V and λ_J , which scale (V_{ij}, J_{ij}) as $(\lambda_V V_{ij}, \lambda_J J_{ij})$. We calculate the spin structure factors of the Hamiltonians for $\lambda_V = 0, 1$ and $\lambda_J = 0, 1$. As shown in Fig. 11, we find that both the off-site Coulomb interactions and the direct exchange interactions significantly reduce the magnetic ordered moment.

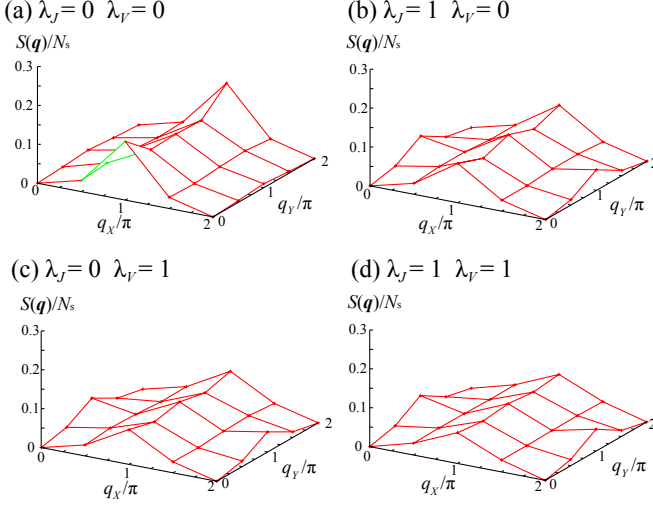


FIG. 11: (color online) Spin structures for (a) $\lambda_J = \lambda_V = 0$ (only on-site Coulomb interaction U), (b) $\lambda_J = 1, \lambda_V = 0$, (c) $\lambda_J = 0, \lambda_V = 1$, and (d) $\lambda_J = \lambda_V = 1$ (*ab initio* Hamiltonian). Both the off-site Coulomb interactions and direct exchange interactions reduce the magnetic ordered moment.

-
- [1] L. Balents, *Nature* **464**, 199 (2010).
- [2] P. W. Anderson, *Materials Research Bulletin* **8**, 153 (1973).
- [3] P. Fazekas and P. W. Anderson, *Philosophical Magazine* **30**, 423 (1974).
- [4] L. Savary and L. Balents, *Reports on Progress in Physics* **80**, 016502 (2016).
- [5] *Frustrated Spin Systems*, ed. H. Diep (World Scientific, Singapore, 2005).
- [6] K. Kanoda and R. Kato, *Annu. Rev. Condens. Matter Phys.* **2**, 167 (2011).
- [7] B. Powell and R. H. McKenzie, *Reports on Progress in Physics* **74**, 056501 (2011).
- [8] Y. Shimizu, K. Miyagawa, K. Kanoda, M. Maesato, and G. Saito, *Phys. Rev. Lett.* **91**, 107001 (2003).
- [9] M. Tamura and R. Kato, *Journal of Physics: Condensed Matter* **14**, L729 (2002).
- [10] T. Itou, A. Oyamada, S. Maegawa, and R. Kato, *Nature Physics* **6**, 673 (2010).
- [11] T. Isono, H. Kamo, A. Ueda, K. Takahashi, M. Kimata, H. Tajima, S. Tsuchiya, T. Terashima, S. Uji, and H. Mori, *Phys. Rev. Lett.* **112**, 177201 (2014).
- [12] M. Yamashita, N. Nakata, Y. Senshu, M. Nagata, H. M. Yamamoto, R. Kato, T. Shibauchi, and Y. Matsuda, *Science* **328**, 1246 (2010).
- [13] P. Bourgeois-Hope, F. Laliberté, E. Lefrançois, G. Griesonanche, S. R. de Cotret, R. Gordon, S. Kitou, H. Sawa, H. Cui, R. Kato, et al., *Phys. Rev. X* **9**, 041051 (2019).
- [14] J. M. Ni, B. L. Pan, B. Q. Song, Y. Y. Huang, J. Y. Zeng, Y. J. Yu, E. J. Cheng, L. S. Wang, D. Z. Dai, R. Kato, et al., *Phys. Rev. Lett.* **123**, 247204 (2019).
- [15] M. Yamashita, *J. Phys. Soc. Jpn.* **88**, 083702 (2019).
- [16] M. Yamashita, Y. Sato, T. Tominaga, Y. Kasahara, S. Kasahara, H. Cui, R. Kato, T. Shibauchi, and Y. Matsuda, *Phys. Rev. B* **101**, 140407(R) (2020).
- [17] K. Nakamura, Y. Yoshimoto, and M. Imada, *Phys. Rev. B* **86**, 205117 (2012).
- [18] E. P. Scriven and B. J. Powell, *Phys. Rev. Lett.* **109**, 097206 (2012).
- [19] A. C. Jacko, L. F. Tocchio, H. O. Jeschke, and R. Valentí, *Phys. Rev. B* **88**, 155139 (2013).
- [20] R. Kato, *Chem. Rev.* **104**, 5319 (2004).
- [21] T. Miyazaki and T. Ohno, *Phys. Rev. B* **68**, 035116 (2003).
- [22] T. Miyazaki and T. Ohno, *Phys. Rev. B* **59**, R5269 (1999).
- [23] T. Tsumuraya, H. Seo, M. Tsuchiizu, R. Kato, and T. Miyazaki, *J. Phys. Soc. Jpn* **82**, 033709 (2013).
- [24] M. Kawamura, K. Yoshimi, T. Misawa, Y. Yamaji, S. Todo, and N. Kawashima, *Comput. Phys. Commun.* **217**, 180 (2017).
- [25] E. Dagotto and A. Moreo, *Phys. Rev. B* **39**, 4744 (1989).
- [26] D. Poilblanc, E. Gagliano, S. Bacci, and E. Dagotto, *Phys. Rev. B* **43**, 10970 (1991).
- [27] T. Misawa, K. Nakamura, and M. Imada, *J. Phys. Soc. Jpn.* **80**, 023704 (2011).
- [28] H. Seo, S. Ishibashi, Y. Otsuka, H. Fukuyama, and K. Terakura, *J. Phys. Soc. Jpn.* **82**, 054711 (2013).
- [29] K. Momma and F. Izumi, *Journal of applied crystallography* **44**, 1272 (2011).
- [30] P. Hohenberg and W. Kohn, *Phys. Rev.* **136**, B864 (1964).
- [31] W. Kohn and L. J. Sham, *Phys. Rev.* **140**, A1133 (1965).
- [32] R. Kato and H. Cui, *Crystals* **2**, 861 (2012).
- [33] K. Ueda, T. Tsumuraya, and R. Kato, *Crystals* **8** (2018).
- [34] P. Giannozzi, O. Andreussi, T. Brumme, O. Bunau, M. B. Nardelli, M. Calandra, R. Car, C. Cavazzoni, D. Ceresoli, M. Cococcioni, et al., *Journal of Physics: Condensed Matter* **29**, 465901 (2017).
- [35] J. P. Perdew, K. Burke, and M. Ernzerhof, *Phys. Rev. Lett.* **77**, 3865 (1996).
- [36] K. Nakamura, Y. Yoshimoto, Y. Nomura, T. Tadano, M. Kawamura, T. Kosugi, K. Yoshimi, T. Misawa, and Y. Motoyama, *arXiv preprint arXiv:2001.02351* (2020).
- [37] H. Kino and H. Fukuyama, *J. Phys. Soc. Jpn.* **65**, 2158 (1996).
- [38] F. Aryasetiawan, M. Imada, A. Georges, G. Kotliar, S. Biermann, and A. I. Lichtenstein, *Phys. Rev. B* **70**, 195104 (2004).
- [39] See Supplemental Materials for details of parameters of the low-energy effective models, effects of the constant shift of the interactions parameters, compound-dependence of the spin structure factors, bond-order structure factors, and effects of off-site interactions.
- [40] H. Shinaoka, M. Troyer, and P. Werner, *Phys. Rev. B* **91**, 245156 (2015).
- [41] C. Honerkamp, H. Shinaoka, F. F. Assaad, and P. Werner, *Phys. Rev. B* **98**, 235151 (2018).
- [42] A. Pustogow, M. Bories, A. Löhle, R. Rösslhuber, E. Zhukova, B. Gorshunov, S. Tomić, J. A. Schlueter, R. Hübner, T. Hiramatsu, et al., *Nature materials* **17**, 773 (2018).
- [43] M. Nakamura, *J. Phys. Soc. Jpn.* **68**, 3123 (1999).
- [44] M. Nakamura, *Phys. Rev. B* **61**, 16377 (2000).
- [45] A. Nakao and R. Kato, *J. Phys. Soc. Jpn.* **74**, 2754 (2005).
- [46] H. Seo, T. Tsumuraya, M. Tsuchiizu, T. Miyazaki, and R. Kato, *J. Phys. Soc. Jpn.* **84**, 044716 (2015).
- [47] H.-Y. Yang, A. M. Läuchli, F. Mila, and K. P. Schmidt, *Phys. Rev. Lett.* **105**, 267204 (2010).
- [48] E. P. Kenny, G. David, N. Ferré, A. C. Jacko, and B. J. Powell, *Phys. Rev. Materials* **4**, 044403 (2020).
- [49] A. Szasz, J. Motruk, M. P. Zaletel, and J. E. Moore, *Phys. Rev. X* **10**, 021042 (2020).
- [50] H. Morita, S. Watanabe, and M. Imada, *J. Phys. Soc. Jpn.* **71**, 2109 (2002).
- [51] L. F. Tocchio, A. Parola, C. Gros, and F. Becca, *Phys. Rev. B* **80**, 064419 (2009).
- [52] R. Orús, *Annals of Physics* **349**, 117 (2014).
- [53] F. Becca and S. Sorella, *Quantum Monte Carlo approaches for correlated systems* (Cambridge University Press, 2017).
- [54] T. Misawa, S. Morita, K. Yoshimi, M. Kawamura, Y. Motoyama, K. Ido, T. Ohgoe, M. Imada, and T. Kato, *Comput. Phys. Commun.* **235**, 447 (2019).
- [55] Y. Zhou, K. Kanoda, and T.-K. Ng, *Rev. Mod. Phys.* **89**, 025003 (2017).
- [56] K. Nakamura, Y. Yoshimoto, Y. Nohara, and M. Imada, *Journal of the Physical Society of Japan* **79**, 123708 (2010).